




Article

Synergistic Antibacterial Mechanism of Mannosylerythritol Lipid-A and Lactic Acid on *Listeria monocytogenes* Based on Transcriptomic Analysis

Xiayu Liu ¹, Xinxin Pang ¹, Yansha Wu ¹, Yajing Wu ¹, Ying Shi ¹ , Xinglin Zhang ^{1,2}  and Qihe Chen ^{1,*} 

¹ Department of Food Science and Nutrition, Zhejiang University, Yuhangtang Rd. 866, Hangzhou 310058, China

² College of Agriculture and Forestry, Linyi University, Linyi 276005, China

* Correspondence: chenqh@zju.edu.cn; Tel.: +86-571-86984316

Abstract: Mannosylerythritol lipids-A (MEL-A) is a novel biosurfactant with multiple biological effects. The synergistic antibacterial activity and mechanism of MEL-A and lactic acid (LA) against *Listeria monocytogenes* were investigated. The synergistic effect resulted in a significant increase in the antibacterial rate compared to LA treatment alone. Genome-wide transcriptomic analysis was applied to deeply investigate the synergistic antibacterial mechanism. Gene Ontology (GO) enrichment analysis showed that the synergy between MEL-A and LA affected many potential cellular responses, including the sugar phosphotransferase system, carbohydrate transport, and ribosomes. KEGG enrichment analysis showed that the PTS system and ribosome-related pathways were significantly enriched. In addition, synergistic treatment affected locomotion and membrane-related cellular responses in GO enrichment analysis and carbohydrate metabolism and amino acid metabolism pathways in KEGG enrichment analysis compared to LA treatment alone. The accuracy of the transcriptome analysis results was verified by qPCR ($R^2 = 0.9903$). This study will provide new insights for the prevention and control of *L. monocytogenes*.

Keywords: Mannosylerythritol lipids-A (MEL-A); lactic acid; *Listeria monocytogenes*; RNA-Seq



Citation: Liu, X.; Pang, X.; Wu, Y.; Wu, Y.; Shi, Y.; Zhang, X.; Chen, Q. Synergistic Antibacterial Mechanism of Mannosylerythritol Lipid-A and Lactic Acid on *Listeria monocytogenes* Based on Transcriptomic Analysis. *Foods* **2022**, *11*, 2660. <https://doi.org/10.3390/foods11172660>

Academic Editor: Leilei Yu

Received: 26 July 2022

Accepted: 28 August 2022

Published: 1 September 2022

Publisher's Note: MDPI stays neutral with regard to jurisdictional claims in published maps and institutional affiliations.



Copyright: © 2022 by the authors. Licensee MDPI, Basel, Switzerland. This article is an open access article distributed under the terms and conditions of the Creative Commons Attribution (CC BY) license (<https://creativecommons.org/licenses/by/4.0/>).

1. Introduction

Foodborne diseases caused by foodborne pathogens are one of the important factors affecting food safety and human health [1]. *L. monocytogenes* is a representative Gram-positive foodborne pathogen that can cause severe meningitis, sepsis, and pregnancy loss primarily in immunocompromised individuals, with a fatality rate as high as 20–30% [2]. Most fatal cases of listeriosis are primarily through the ingestion of contaminated processed food products, raw meat, sea food, dairy products, etc. [3]. *L. monocytogenes* can also utilize a plethora of complex regulatory mechanisms (e.g., riboregulators and small non-coding RNAs) to rapidly adapt to different extreme environments and can traverse different epithelial barriers to cause host infection [2,4]. Hence, the exploration of biochemical agents that effectively inhibit the growth and survival of *L. monocytogenes* is crucial for food safety.

Lactic acid is a “Generally Recognized as Safe” (GRAS) food additive and has been widely used for the control of pathogenic bacteria in perishable foods such as meat and dairy products due to its simple process, significant antibacterial effect, and low price [5,6]. LA has been reported to have significant antibacterial activity against pathogens such as *Salmonella enterica*, *Escherichia coli*, and *L. monocytogenes* [7]. Previous studies have shown that LA can lead to the destruction of the membrane structure and intracellular structure of pathogenic bacteria and the leakage of proteins, affecting the physiological and morphological changes of bacterial cells to play an antibacterial effect [7,8]. However, due to the complexity of the composition of real food systems and the strong tolerance of *L. monocytogenes*, a high addition level is often required to effectively inhibit *L. monocytogenes* in food systems [9].

Moreover, the addition of LA at high levels may affect the color, sensorial properties, and commercial characteristics of food products [10]. Therefore, *L. monocytogenes* can be effectively controlled in real food systems through the synergistic use of antimicrobial agents, while reducing the concentration of individual use [11].

Mannosylerythritol lipids (MELs) are glycolipid biosurfactants mainly produced by yeast strains of the genus *Pseudozyma* [12]. Depending on the degree of acetylation, MELs can be classified into four different conformations, including MEL-A, MEL-B, MEL-C, and MEL-D [13]. MELs exhibit not only excellent interfacial activity and biodegradability, but also biochemical activities such as antioxidant, antibacterial, anti-inflammatory, and anticancer [14]. In terms of antibacterial activity, our previous studies showed that MELs exhibited excellent inhibitory effects on Gram-positive pathogens such as *Staphylococcus aureus* and *Bacillus cereus* [15–17]. In terms of the antibacterial mechanism, our previous studies have shown that MEL-A has a significant damaging effect on the cell membrane of pathogenic bacteria, causing the leakage of intracellular nucleic acids and proteins and affecting the expression of the ABC transport system and membrane-related genes [16,18]. In addition, studies have shown that MEL-A can significantly improve the antibacterial activity against methicillin-resistant *Staphylococcus aureus* (MRSA) in the biofilm state and *L. monocytogenes* in the planktonic state by synergistic treatment with physical means, such as ultrasound and ultrahigh pressure [19,20].

There are also differences in the gene expression and regulation patterns of bacteria under different stresses. For instance, a pulsed magnetic field (PMF) can lead to the death of *L. monocytogenes* primarily through disruption of biological functions (phosphorylation and dephosphorylation, membrane, quorum sensing, etc.) and metabolism (carbohydrate metabolism, energy metabolism, amino acid metabolism, etc.) [21]. Fingered Citron essential oil exerts anti-listeria activity mainly by affecting chemotaxis and flagellar assembly as well as carbohydrate and metal cation uptake [22]. Furthermore, the regulation of genes under the same stress may have strain differences [23]. However, the synergistic antibacterial activity of MEL-A with chemical agents has been little explored. Therefore, in this study, we focused on the synergistic antibacterial activity of MEL-A and LA against *L. monocytogenes* EGD-e, a representative 1/2a serotype associated with human infection [24] and explored the antibacterial mechanism of synergistic processing through genome-wide transcriptomic analysis.

2. Materials and Methods

2.1. Bacterial Strains and Chemical Reagents

L. monocytogenes EGD-e (ATCC BAA-679, serovar 1/2a) was purchased from the American Type Culture Collection (ATCC, Manassas, VA, USA). Unless otherwise mentioned, *L. monocytogenes* was cultured in brain heart infusion (BHI) or BHI agar (Hopebiol, Qingdao, China) at 37 °C. Lactic acid (purity, over 98%, CAS 79-33-4) was purchased from Aladdin (Shanghai, China) and dissolved in sterile water. MEL-A was produced by our laboratory according to the previous method [18,19,25].

2.2. Synergistic Antibacterial Activity Assessment

To evaluate the synergistic antibacterial activity of MEL-A and LA against *L. monocytogenes*, 50 mL of BHI with different concentrations of LA (0, 1, and 2 mg/mL) and MEL-A (0 and 32 µg/mL) was prepared. Then, logarithmic growth stage *L. monocytogenes* was harvested, washed 3 times (4000× g, 2 min, 37 °C) with phosphate-buffered saline (PBS, 20 mM, pH 7.4), and diluted to obtain a final inoculum of 10⁶ CFU/mL as seeds. Next, 1 mL of *L. monocytogenes* (1.0 × 10⁶ CFU/mL) seed solution was inoculated into shaking flasks (50 mL BHI), and all flasks were incubated in an orbital shaker (180 rpm at 37 °C) (Thermo Fisher Scientific, Waltham, MA, USA). Then, 100 µL of bacterial suspension was removed from the flasks after 24 h, respectively, and the gradient dilution was spread evenly on BHI plates and incubated in an incubator (Thermo Fisher Scientific, Waltham, MA, USA) at 37 °C. *L. monocytogenes* was counted by the plate count method, and the amount of

bacteria was expressed as CFU/mL. The antibacterial rate was calculated according to the following formula:

$$R (\%) = (C - E) / C \times 100\% \quad (1)$$

where R: antibacterial rate (%); C: number of bacteria in the control group (CFU/mL); and E: the number of bacteria in the experimental group (CFU/mL).

2.3. RNA Isolation and Sequencing

Approximately 1×10^6 CFU of *L. monocytogenes* was incubated in BHI and BHI supplemented with MEL-A (32 μ g/mL) and LA (2 mg/mL) at 37 °C for 12 h. Bacterial cells were then collected by centrifugation at $2500 \times g$ for 5 min and then snap-frozen in liquid nitrogen. Next, total RNA was extracted using the method described by Kafantaris [26]. Then, total RNA from all samples was sent to Novogene company (Beijing, China) for subsequent library construction and transcription sequencing. Briefly, the libraries were constructed using the NEBNext[®] UltraTM RNA Library Prep Kit (New England Biolabs, Los Angeles, CA, USA) according to the manufacturer's instructions. Then, these libraries were sequenced on the Illumina Novaseq platform (Illumina, San Diego, CA, USA) and 150 bp paired-end readings were generated. Three biological replicates were performed in both the experimental group and the control group. Next, in-house perl scripts were used to process raw data (raw reads) in fastq format. The next step was to remove readings containing an adapter, readings containing N bases, and readings of low quality from the raw data in order to obtain clean data (clean readings). Furthermore, Q20, Q30, and GC content clean data were calculated. All downstream analyses relied on clean data.

2.4. Differential Expression Analysis

Differential expression analysis was performed using the DESeq R package (1.20) (Sydney, NSW, Australia). The DESeq program provides statistical routines for analyzing digital gene expression data using a negative binomial distribution model. Using Benjamini-Hochberg's approach, we adjusted the resulting *p*-values for false discovery. Differentially expressed genes were identified by DESeq with an adjusted *p*-value of 0.05.

2.5. GO and KEGG Analysis of Differential Gene Expression

GO enrichment analysis of differentially expressed genes was implemented by the GOseq R package (Beijing, China). The differentially expressed genes were considered significantly enriched for GO terms with corrected *p*-values less than 0.05. KOBAS software (Beijing, China) was used to test the statistical enrichment of differentially expressed genes in KEGG pathways.

2.6. Real-Time qPCR Analysis

Eight genes with significant regulations were selected for RT-qPCR analysis. A Prime-Script RT reagent Kit with gDNA Eraser (Takara, Osaka, Japan) was used to synthesize cDNA. Next, real-time PCR analysis on these cDNA was performed using the TB Green[®] Premix Ex Taq[™] (Tli RNaseH Plus) Kit (Thermo Fisher Scientific, Waltham, MA, USA) and the Applied Biosystems[™] QuantStudio[™] 3 instrument (Thermo Fisher Scientific, Waltham, MA, USA). As an internal reference gene, *drm* was used. Data analysis was carried out using the $2^{-\Delta\Delta C_t}$ method [27] with 3 biological replicates per group.

2.7. Statistical Analysis

Data were presented as mean \pm standard deviation. All experiments were analyzed using one-way analysis of variance (ANOVA) and Duncan's multiple range test (DMRT). Tests were run in triplicate, and statistical significance was defined as $p < 0.05$.

3. Results and Discussion

3.1. Synergistic Antibacterial Activity of MEL-A and LA on *L. monocytogenes*

Our previous study [18] showed that MEL-A inhibited *L. monocytogenes* significantly when added at a concentration of 32 µg/mL; therefore, we chose 32 µg/mL as the addition concentration in this study. As shown in Table 1, when LA was 1 mg/mL, the addition of MEL-A could increase the antibacterial rate from 50.0% to 99.4%, and when LA was 2 mg/mL, the antibacterial rate increased from 89.4% to 99.9%; the results also showed that there was a concentration-dependent effect of LA. Previous studies have shown that the Minimal inhibitory concentrations (MIC) of LA alone against *L. monocytogenes* is 5000 µg/mL (0.5%) [28]. Therefore, the addition of MEL-A can significantly reduce the use of LA and reduce the impact on food quality. In conclusion, the synergistic treatment of MEL-A and LA significantly improved the antibacterial effect on *L. monocytogenes*.

Table 1. Synergistic antibacterial activity of MEL-A and LA on *L. monocytogenes*.

Treatment	Log (CFU/mL)	Log Reduction (CFU/mL)	Antibacterial Rate (%)
Control	9.44 ± 0.01 ^a	—	—
MEL-A (32 µg/mL)	8.70 ± 0.03 ^c	0.74	81.8
LA (1 mg/mL)	9.13 ± 0.10 ^b	0.31	50.0
LA (1 mg/mL) + MEL-A (32 µg/mL)	7.14 ± 0.26 ^e	2.30	99.4
LA (2 mg/mL)	8.46 ± 0.04 ^d	0.98	89.4
LA (2 mg/mL) + MEL-A (32 µg/mL)	6.45 ± 0.09 ^f	2.99	99.9

Statistically significant differences ($p < 0.05$) are indicated by letters above each column (mean ± standard deviation).

3.2. Effect of Synergistic Effect of MEL-A and LA on the Transcriptome Profile of *L. monocytogenes*

3.2.1. Global Response of *L. monocytogenes* to the Synergistic Treatment (ML Group)

Transcriptomic analysis was performed to further study the synergistic antibacterial mechanism of MEL-A and LA against *L. monocytogenes*. As shown in Figure 1A, the squares of the Pearson correlation coefficients (R^2) of different samples between the same group were greater than 0.96, which indicated a very high similarity of expression patterns between samples [29]. In the principal component analysis (PCA), 93.67% of the difference between the two groups came from PC1 and 2.04% of the difference came from PC2, indicating that the synergistic treatment group had a significant difference against *L. monocytogenes* compared to the control (Figure 1B). In addition, significant differences in the heat map (Figure 1C) between the two groups also indicated significant differences in expression patterns between the synergistic treatment group and the control group.

As shown in Figure 1D, a total of 1563 genes were identified as differentially expressed genes (DEGs), of which 756 were up-regulated and 807 were down-regulated (Table S1). In the synergistic treatment group, the genes *lmo2185* (log₂FC 10.68), *lmo1250* (log₂FC 9.49), *lmo2186* (log₂FC 9.05), *lmo2180* (log₂FC 8.90), *lmo1007* (log₂FC 8.42), *lmo1958* (log₂FC 8.42), *lmo2181* (log₂FC 8.17), and *lmo2183* (log₂FC 7.88) were among the top up-regulated genes. These genes mainly encode the antibiotic resistance protein, the ferri-chrome ABC transporter permease, and the hypothetical protein, and they mainly belong to the Iron Transport-associated domain, Major Facilitator Superfamily (MFS), and FecCD transport family. Iron acquisition and utilization by *L. monocytogenes* is important not only for infection but also for growth and survival in diverse environments [30,31]. Furthermore, MFS transporters are also reported to be involved in the transmembrane uptake of small molecules and the excretion of harmful compounds [32]. Together, these findings suggest that the synergistic processing of MEL-A and LA may hinder the transmembrane transport of small molecules such as iron by bacteria, resulting in a decrease in bacterial viability.

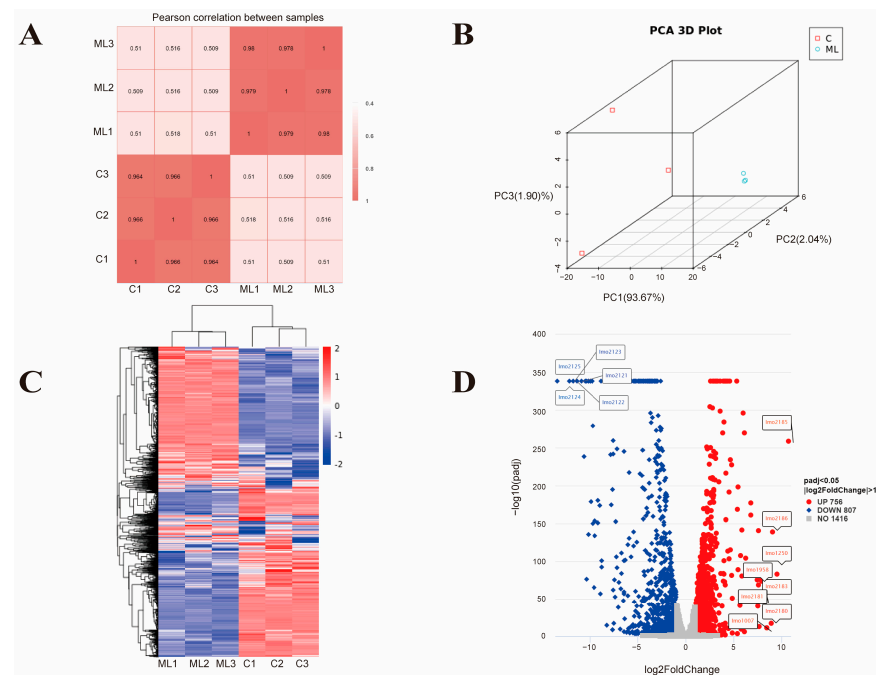


Figure 1. Gene expression patterns of control and ML. **(A)** Gene expression correlation graph. **(B)** Principal component analysis (PCA) graph of gene expression. **(C)** Heat map of DEGs ($|\log_2FC| > 1$ and $P_{adj} < 0.05$). **(D)** Volcano plot of the DEGs ($|\log_2FC| > 1$ and $P_{adj} < 0.05$). Each dot represents a gene, and the up-regulated and down-regulated genes with the largest fold change are marked in the graph. Fold change is represented on the x-axis, while p adjust is represented on the y-axis. Red and blue indicate differentially up-regulated and differentially down-regulated genes, respectively, while gray dots indicate genes that were not significantly different from the control group.

The most significantly down-regulated genes mainly included an operon from *lmo2121* to *lmo2125* (\log_2FC ranged from -10.94 to -13.44). These genes mainly encode the maltose phosphorylase, maltodextrone utilization protein MalA, sugar ABC transporter permease, and sugar ABC transporter substrate-binding protein. These findings suggest that synergistic treatment can inhibit the sugar transport and utilization (which are reported to be critical for bacterial energy supply and growth) [33] of *L. monocytogenes*. Therefore, this may be another important reason for the synergistic effect of MEL-A and LA on *L. monocytogenes*.

3.2.2. GO Enrichment Analysis of the ML Group and the Control Group

Our first step was to perform GO enrichment analysis in order to better understand the biological function of DEGs. The top 20 enriched GO terms of DEGs are shown in Figure 2. The most significantly enriched GO terms were “phosphoenolpyruvate-dependent sugar phosphotransferase system” in the Biological Processes (BP) category, “protein-N(PI)-phosphohistidine-sugar phosphotransferase activity” in the Molecular Function (MF) category, and “ribosome” in the Cellular Component (CC) category. The sugar phosphotransferase system has been reported to not only play a crucial role in carbohydrate uptake but also to control carbon and nitrogen metabolism, biofilm formation, and other bacterial responses to changing environmental conditions through a highly complex carbohydrate sensor system [34,35]. In addition, ribosome-related genes are also frequently identified under extreme environmental conditions (including acidity, low temperature, and high pressure, etc.) [19,36,37]. In detail, in the CC category, the most significantly enriched GO terms were “ribosome”, “intracellular ribonucleoprotein complex”, and “ribonucleoprotein complex” in the up-regulated genes (Figure S1A) and “bacterial-type flagellum” and “cell projection” in the down-regulated genes (Figure S1D). In the MF category, the most significantly enriched GO terms were “structural constituent of ribosome”, “structural molecule activity”, and “GTP binding” in the up-regulated genes (Figure S1B)

and “protein-N(PI)-phosphohistidine-sugar phosphotransferase activity”, “carbohydrate transmembrane transporter activity”, and “carbohydrate transporter activity” in the down-regulated genes (Figure S1E). Moreover, in the BP category, the most significantly enriched GO terms were “cellular amide metabolic process”, “translation”, and “amide biosynthetic process” in the up-regulated genes (Figure S1C) and “phosphoenolpyruvate-dependent sugar phosphotransferase system”, “carbohydrate transport”, and “organic substance transport” in the down-regulated genes (Figure S1F).

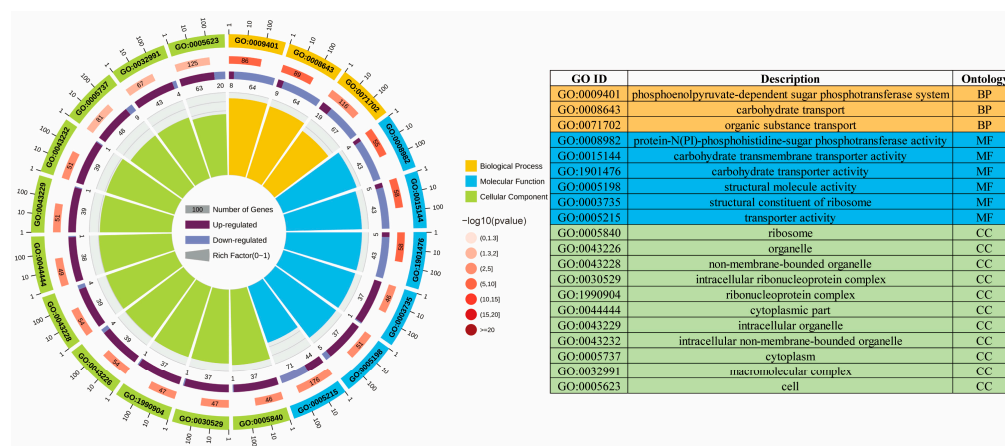


Figure 2. GO enrichment analysis of the ML group and the control. There are four circles from the outside to the inside. The first circle shows the classification of enrichment. Outside the circle is a coordinate ruler showing the number of genes. Each color represents a different category. On the second circle, the category number and the p -value are shown. A larger number of genes, a longer bar, and a smaller value results in a redder color. In the third circle, you can see the ratio of genes that are up-regulated and down-regulated; dark purple represents up-regulated genes, and light purple represents down-regulated genes. The fourth circle: the Rich Factor represents the number of foreground genes in each category divided by the number of background genes, while each cell on the background auxiliary line represents 0.1.

3.2.3. KEGG Pathway Enrichment Analysis of the ML Group and the Control Group

KEGG pathway enrichment analysis was conducted for further in-depth analysis of DEGs. From the overall pathway, the synergistic processing of MEL-A and LA significantly affected the phosphotransferase system (PTS), ribosomes, and multiple metabolism-related pathways (including fructose and mannose metabolism, starch and sucrose metabolism, and amino sugar and nucleotide sugar metabolism, etc.) (Figure 3A). In addition, these pathways are closely related each other (Figure 3B). Specifically, among the up-regulated genes, the most significantly enriched KEGG B-level pathways were membrane transport, carbohydrate metabolism, and translation (Figure S2A), while subdivided into metabolic pathways were ribosomes, fatty acid metabolism, fatty acid biosynthesis, and ABC transporters (Figure S2B). Among the down-regulated genes, the most significantly enriched KEGG B-level pathways were membrane transport, carbohydrate metabolism, and energy metabolism (Figure S2C), while subdivided into metabolic pathways were phosphotransferase system (PTS), fructose, mannose metabolism, and starch and sucrose metabolism (Figure S2D).

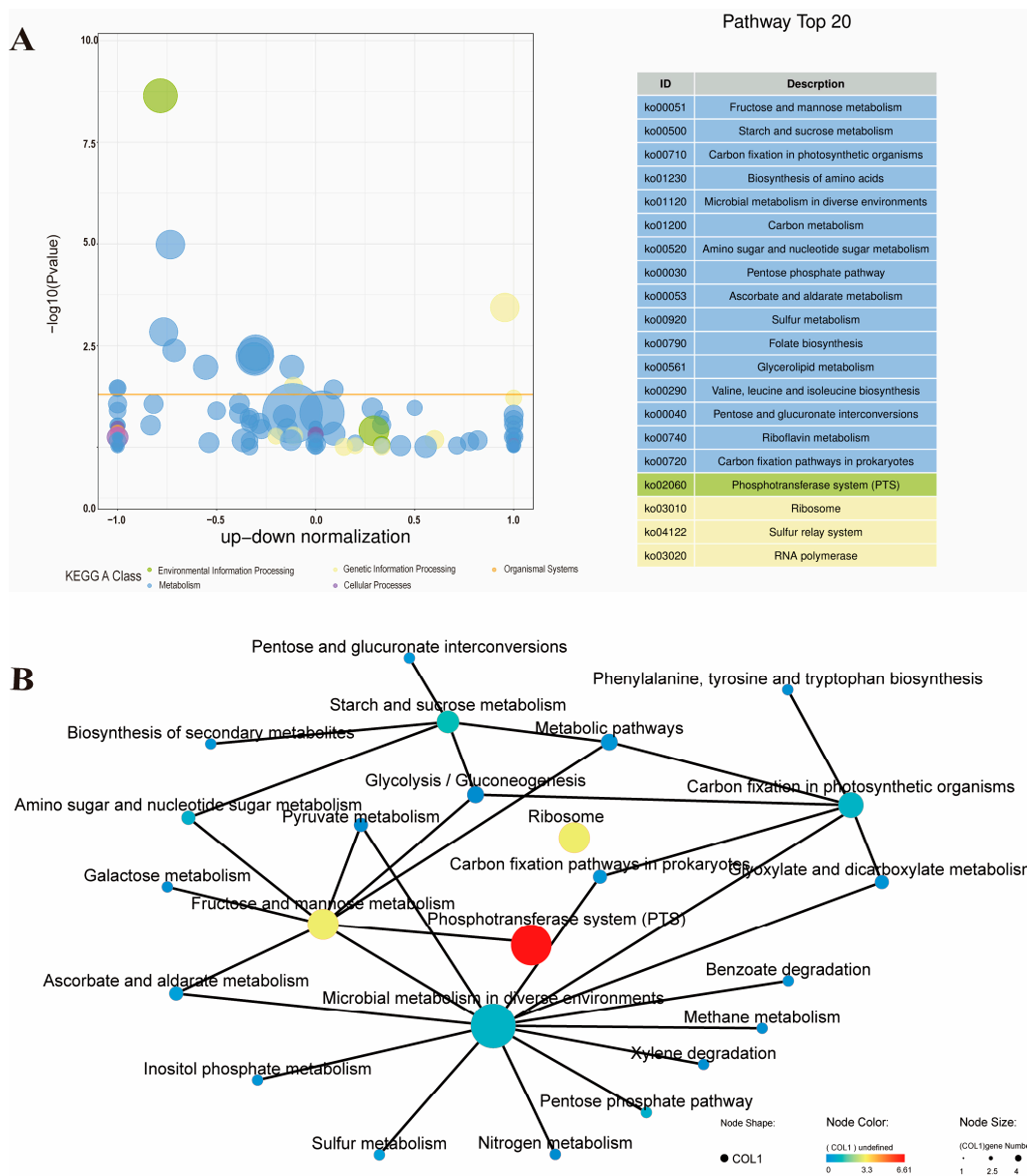


Figure 3. KEGG enrichment analysis of the ML group and the control. **(A)** Bubble plot of the top 20 KEGG enriched pathways. The horizontal axis of the bubble chart is the normalization coefficient of up and down; the vertical axis is $-\log_{10}P$ value. Different colors represent KEGG A classification of different pathways, and the orange threshold line is p -value = 0.05. Genes enriched by the current pathway are represented by the size of the bubble. The table on the right shows the 20 KEGG pathways with the smallest p -values. **(B)** Pathway networks enriched with KEGG annotations. The KEGG pathway is represented by nodes of different colors and sizes, with the size of the node representing the number of genes enriched in the pathway, and the gradient color of the node represents the p -value of the KEGG enrichment analysis; the solid line represents the connection between the pathway and the pathway or between the pathway and the gene. An isolated node in the graph indicates that the pathway is not directly related to other pathways in the graph.

In this study, the ribosome was the most significantly up-regulated pathway in the KEGG enrichment analysis. The 70S ribosome of bacteria consists of a large subunit (50S) and a small subunit (30S). The large subunit contains 23S RNA, 5S RNA, and more than 30 kinds of proteins, and the small subunit contains 16S RNA and more than 20 kinds of proteins [38]. Previous studies have shown that ribosomes, as the hub of protein quality control whose main function is to convert the genetic code into amino acid sequences

and build protein polymers from amino acid monomers, are essential for bacterial protein synthesis and normal life activities [39]. In addition, studies have found that many clinically useful antibiotics exert their antibacterial effects by blocking protein synthesis on bacterial ribosomes, and people have begun to artificially design some ribosome-targeting antibiotics [40,41]. Therefore, the general up-regulation of ribosome-related genes (Figure 4A) caused by the synergistic processing of MEL-A with LA suggests that the effect on the protein synthesis process of the ribosome may be an important reason for its synergistic antibacterial activity.

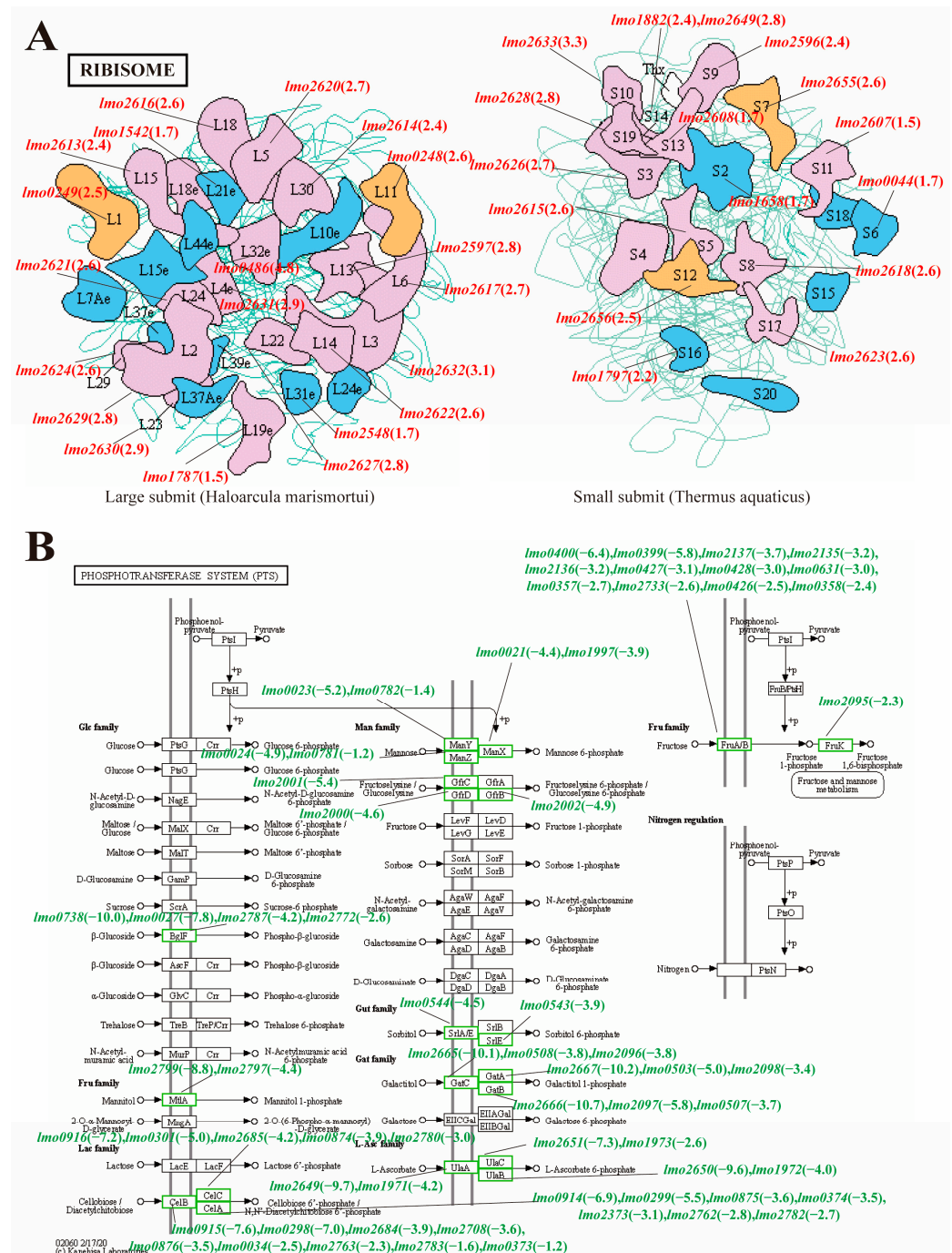


Figure 4. KEGG pathway analysis of ribosomes (A) and PTS (B). The red fonts in the figure represent significantly up-regulated genes in related pathways, and the green fonts represent significantly down-regulated genes in related pathways.

The phosphotransferase system (PTS) was the most significantly down-regulated pathway in the KEGG enrichment analysis. In bacteria, PTS not only catalyzes sugar transport and sugar phosphorylation, but it also regulates various transport, metabolic, and mutagenesis processes and the expression of numerous genes [42]. Many previous studies have shown that PTS is one of the key targets of many antibacterial agents [43–45]. As shown in Figure 4B, the synergistic treatment of MEL-A and LA also led to the downregulation of a large number of PTS-related genes, indicating that the effect of synergistic treatment on PTS sugar transport and sugar phosphorylation is also one of the important reasons for its inhibition of *L. monocytogenes*. These results are also consistent with our previous findings [19].

In this study, we selected *L. monocytogenes* EGD-e, a representative 1/2a serotype associated with human infection, for further study. However, there may be differences in the antibacterial mechanisms among strains [23], so subsequent studies could be conducted for comparative analysis of multiple strains. Moreover, previous studies have shown that both MEL-A and LA have significant damaging effects on the cell membrane structure of pathogenic bacteria and lead to the leakage of intracellular nucleic acids and proteins [7,8,16,18]. Therefore, the significant antibacterial activity of MEL-A and LA co-treatment against *L. monocytogenes* may be mainly due to the superimposed effect on the membrane structure and intracellular macromolecular substances.

3.3. Comparative Transcriptome Analysis of the ML Co-Treatment Group and the LA Treatment Group Alone

To further explore the addition of MEL-A on the antibacterial mechanism of *L. monocytogenes* compared with LA treatment alone, we also performed GO and KEGG enrichment analysis of the DEGs in the ML group and the LA group. In the GO enrichment analysis, locomotion-related biological processes and membrane-related (including integral components of membranes, intrinsic components of membranes, integral components of plasma membranes, intrinsic components of plasma membranes, membranes, etc.) cellular components were significantly enriched (Figure 5A). In addition, in the secondary classification of GO terms, biological processes related to metabolic processes, cellular components related to membranes, and molecular functions related to catalytic activity contained the largest number of DEGs (Figure 5B). The destruction of cell membrane structures by MEL-A has also been confirmed in our previous microstructure observation and biochemical index determination, which may be one of the key mechanisms of its antibacterial effect [14,19]. In addition, the general downregulation of locomotion-related genes indicated that MEL-A significantly reduced the motility of *L. monocytogenes*, thereby hindering its growth and reproduction process. In the KEGG enrichment analysis, pathways related to carbohydrate metabolism (butanoate metabolism, inositol phosphate metabolism, etc.) and amino acid metabolism (phenylalanine, tyrosine, and tryptophan biosynthesis, etc.) were significantly enriched. These results demonstrated that cells required carbohydrates and amino acids to repair damage caused by MEL-A treatment [21].

3.4. RT-qPCR Validation of RNA-Seq Data

As shown in Figure 6, we analyzed the transcription level of *lmo0248*, *lmo0249*, *lmo2623*, *lmo2628*, *lmo2123*, *lmo2124*, *lmo2347*, and *lmo2348* by real-time quantitative PCR to verify the accuracy of the transcriptome data. It was highly consistent between the RNA-Seq and qPCR results ($R^2 = 0.9903$), which demonstrated the reliability of our transcriptome data.

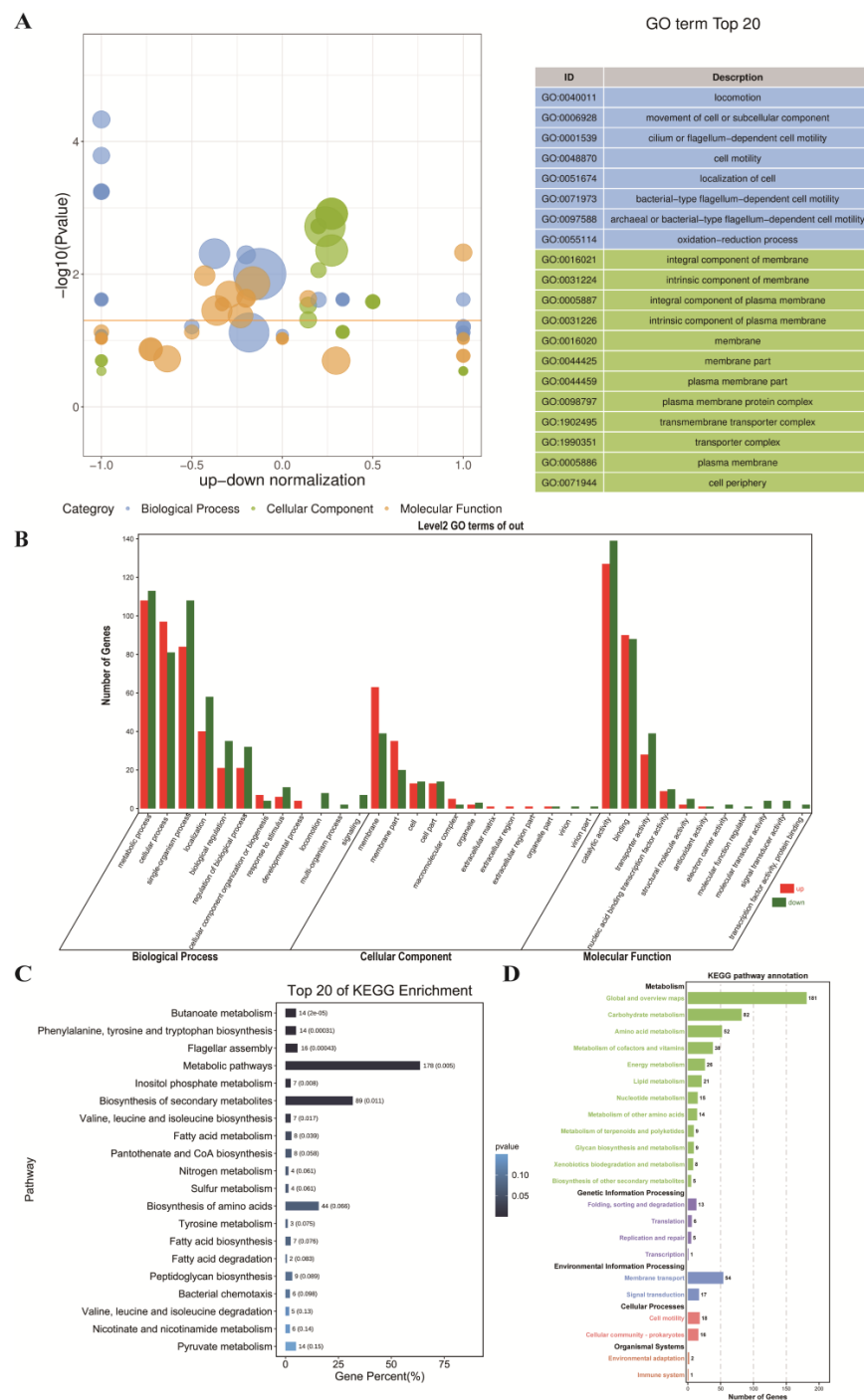


Figure 5. GO enrichment analysis (A,B) and KEGG enrichment analysis (C,D) of the ML co-treatment group and the LA treatment group. (A) Regarding the z-score bubble chart of GO enrichment analysis, the ordinate is $-\log_{10}(p\text{ value})$, and the abscissa is the up-down normalization value (the ratio of the difference between the number of differentially up-regulated genes and the number of differentially down-regulated genes to the total differential genes). The size of the bubble represents the number of target genes enriched by the current GO term; the yellow line represents the threshold of $p\text{-value} = 0.05$; the right side is the list of the top 20 terms with the $p\text{-value}$, and different colors represent different Ontologies. (B) Statistical plot of secondary classifications for GO enrichment analysis. The abscissa is the different GO terms, and the ordinate is the number of target genes enriched by the current GO term. Genes that are up-regulated are represented by red, while genes that are down-regulated are represented by green. (C) Bar graph of the top 20 significantly enriched pathways. (D) Statistical chart of the B-class classification for each pathway.

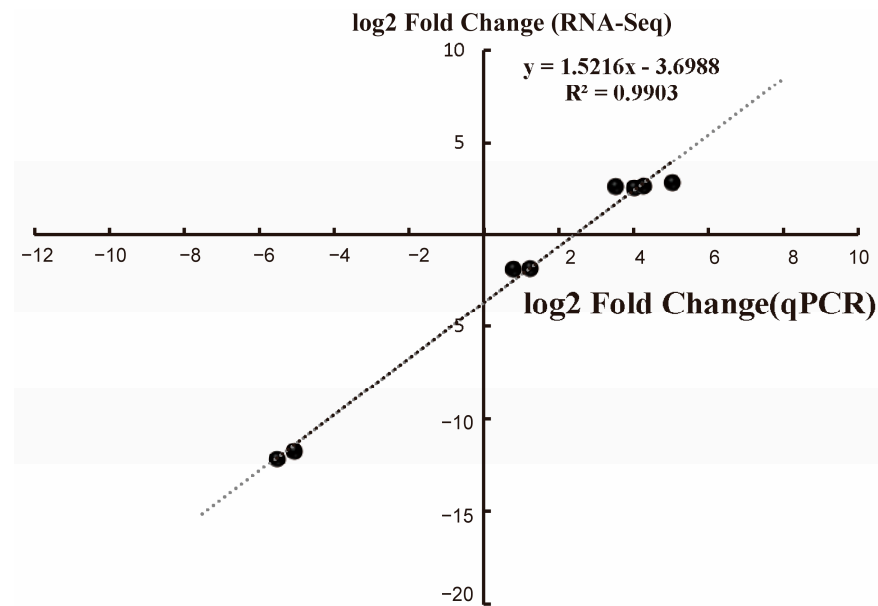


Figure 6. RT-qPCR validation of RNA-Seq results for the ML treatment groups. Three biological replicates were performed for each group. The horizontal coordinate is the log₂ Fold Change value obtained from qPCR data and the vertical coordinate is the log₂ Fold Change value obtained from RNA-Seq data.

4. Conclusions

In this study, the synergistic antibacterial effect of LA with a novel biosurfactant MEL-A was investigated. In addition, the gene expression changes of *L. monocytogenes* after synergistic treatment were evaluated by transcriptomics to reveal the synergistic antibacterial mechanism. Specifically, GO enrichment and KEGG pathway analysis demonstrated significant changes in sugar phosphotransferase system, carbohydrate transport, and ribosomes. Interestingly, synergistic treatment of MEL-A with LA also affected locomotion and membrane-related GO terms as well as carbohydrate metabolism and amino acid metabolism-related pathways, compared with LA treatment alone. Overall, these findings provide new insights into the synergistic antibacterial mechanisms of MEL-A and LA on *L. monocytogenes* and may contribute to the development of novel strategies against *L. monocytogenes* in the food industry.

Supplementary Materials: The following supporting information can be downloaded at: <https://www.mdpi.com/article/10.3390/foods11172660/s1>, Table S1: DEGs in the co-treated group of MEL-A and LA. Figure S1: Bubble plot of GO enrichment analysis for ML group and control. Figure S2: KEGG histogram enrichment analysis of ML group and control.

Author Contributions: Conceptualization, X.L. and X.Z.; methodology, X.L., X.P., Y.W. (Yansha Wu), and Y.W. (Yajing Wu); formal analysis, X.L., X.Z., Q.C., and Y.S.; investigation, X.L., X.P., Y.W. (Yansha Wu), Y.W. (Yajing Wu), and Y.S.; data curation, X.L. and X.P.; writing—original draft preparation, X.L. and X.Z.; writing—review and editing, X.L., X.Z., Q.C., and Y.S.; funding acquisition, X.Z. All authors have read and agreed to the published version of the manuscript.

Funding: This work was supported by the National Key Research and Development Program of China [2019YFE0103900], the Natural Science Foundation of Shandong Province, China [ZR2019ZD21], the Taishan Scholars Program of Shandong Province, China [ts20190955], and the Project of Shandong Province Higher Educational Outstanding Youth Innovation Team [2019KJF011].

Institutional Review Board Statement: Not applicable.

Informed Consent Statement: Not applicable.

Data Availability Statement: The raw RNA-seq data are available at NCBI Sequence Read Archive (NCBI SRA) under BioProject accession no. PRJNA862260. <https://dataview.ncbi.nlm.nih.gov/object/PRJNA862260?reviewer=jgmc3drj6q4jpdgd91u0qeq>.

Conflicts of Interest: The authors declare no conflict of interest.

References

- Liu, X.; Liu, G.; Wu, Y.; Pang, X.; Wu, Y.; Qinshu; Niu, J.; Chen, Q.; Zhang, X. Transposon sequencing: A powerful tool for the functional genomic study of food-borne pathogens. *Trends Food Sci. Technol.* **2021**, *118*, 679–687. [\[CrossRef\]](#)
- Radoshevich, L.; Cossart, P. *Listeria monocytogenes*: Towards a complete picture of its physiology and pathogenesis. *Nat. Rev. Microbiol.* **2018**, *16*, 32–46. [\[CrossRef\]](#) [\[PubMed\]](#)
- Zhu, Q.; Gooneratne, R.; Hussain, M.A. *Listeria monocytogenes* in Fresh Produce: Outbreaks, Prevalence and Contamination Levels. *Foods* **2017**, *6*, 21. [\[CrossRef\]](#) [\[PubMed\]](#)
- Cossart, P. Illuminating the landscape of host-pathogen interactions with the bacterium *Listeria monocytogenes*. *Proc. Natl. Acad. Sci. USA* **2011**, *108*, 19484–19491. [\[CrossRef\]](#)
- Ozdemir, H.; Yildirim, Y.; Kuplulu, O.; Koluman, A.; Goncuoglu, M.; Inat, G. Effects of lactic acid and hot water treatments on *Salmonella Typhimurium* and *Listeria monocytogenes* on beef. *Food Control* **2006**, *17*, 299–303. [\[CrossRef\]](#)
- Byelashov, O.A.; Daskalov, H.; Geornaras, I.; Kendall, P.A.; Belk, K.E.; Scanga, J.A.; Smith, G.C.; Sofos, J.N. Reduction of *Listeria monocytogenes* on frankfurters treated with lactic acid solutions of various temperatures. *Food Microbiol.* **2010**, *27*, 783–790. [\[CrossRef\]](#)
- Wang, C.; Chang, T.; Yang, H.; Cui, M. Antibacterial mechanism of lactic acid on physiological and morphological properties of *Salmonella Enteritidis*, *Escherichia coli* and *Listeria monocytogenes*. *Food Control* **2015**, *47*, 231–236. [\[CrossRef\]](#)
- Lin, C.; Qin, L.; Xue, Z.; Hongfei, Z.; Xinyi, P.; Hongshun, Y. Inactivation efficacies of lactic acid and mild heat treatments against *Escherichia coli* strains in organic broccoli sprouts. *Food Control* **2022**, *133 Pt A*, 108577.
- Gonzalez-Fandos, E.; Martinez-Laorden, A.; Perez-Arnedo, I. Efficacy of combinations of lactic acid and potassium sorbate against *Listeria monocytogenes* in chicken stored under modified atmospheres. *Food Microbiol.* **2021**, *93*, 103596. [\[CrossRef\]](#)
- Capita, R.; Alonso-Calleja, C.; Rodriguez-Perez, R.; Moreno, B.; Garcia-Fernandez, M.D. Influence of poultry carcass skin sample site on the effectiveness of trisodium phosphate against *Listeria monocytogenes*. *J Food Protect.* **2002**, *65*, 853–856. [\[CrossRef\]](#)
- Kozak, S.M.; Margison, K.M.; D’Amico, D.J. Synergistic Antimicrobial Combinations Inhibit and Inactivate *Listeria monocytogenes* in Neutral and Acidic Broth Systems. *J. Food Protect.* **2017**, *80*, 1266–1272. [\[CrossRef\]](#) [\[PubMed\]](#)
- Nashida, J.; Nishi, N.; Takahashi, Y.; Hayashi, C.; Igarashi, M.; Takahashi, D.; Toshima, K. Systematic and Stereoselective Total Synthesis of Mannosylerythritol Lipids and Evaluation of Their Antibacterial Activity. *J. Org. Chem.* **2018**, *83*, 7281–7289. [\[CrossRef\]](#) [\[PubMed\]](#)
- Silva Coelho, A.L.; Feuser, P.E.; Mattar Carciofi, B.A.; de Andrade, C.J.; de Oliveira, D. Mannosylerythritol lipids: Antimicrobial and biomedical properties. *Appl. Microbiol. Biot.* **2020**, *104*, 2297–2318. [\[CrossRef\]](#)
- Shu, Q.; Lou, H.; Wei, T.; Liu, X.; Chen, Q. Contributions of Glycolipid Biosurfactants and Glycolipid-Modified Materials to Antimicrobial Strategy: A Review. *Pharmaceutics* **2021**, *13*, 227. [\[CrossRef\]](#) [\[PubMed\]](#)
- Shu, Q.; Wei, T.; Lu, H.; Niu, Y.; Chen, Q. Mannosylerythritol lipids: Dual inhibitory modes against *Staphylococcus aureus* through membrane-mediated apoptosis and biofilm disruption. *Appl. Microbiol. Biot.* **2020**, *104*, 5053–5064. [\[CrossRef\]](#)
- Shu, Q.; Niu, Y.W.; Zhao, W.J.; Chen, Q.H. Antibacterial activity and mannosylerythritol lipids against vegetative cells and spores of *Bacillus cereus*. *Food Control* **2019**, *106*, 106711. [\[CrossRef\]](#)
- Qin, S.; Tianyu, W.; Xiayu, L.; Siyu, L.; Qihe, C. The dough-strengthening and spore-sterilizing effects of mannosylerythritol lipid-A in frozen dough and its application in bread making. *Food Chem.* **2022**, *369*, 131011.
- Liu, X.; Shu, Q.; Chen, Q.; Pang, X.; Wu, Y.; Zhou, W.; Wu, Y.; Niu, J.; Zhang, X. Antibacterial Efficacy and Mechanism of Mannosylerythritol Lipids-A on *Listeria monocytogenes*. *Molecules* **2020**, *25*, 4857. [\[CrossRef\]](#)
- Liu, X.; Zhang, L.; Pang, X.; Wu, Y.; Wu, Y.; Shu, Q.; Chen, Q.; Zhang, X. Synergistic antibacterial effect and mechanism of high hydrostatic pressure and mannosylerythritol Lipid-A on *Listeria monocytogenes*. *Food Control* **2022**, *135*, 108797. [\[CrossRef\]](#)
- Shu, Q.; Lou, H.; Wei, T.; Zhang, X.; Chen, Q. Synergistic antibacterial and antibiofilm effects of ultrasound and MEL-A against methicillin-resistant *Staphylococcus aureus*. *Ultrason. Sonochemistry* **2021**, *72*, 105452. [\[CrossRef\]](#)
- Qian, J.; Zhang, M.; Dai, C.; Huo, S.; Ma, H. Transcriptomic analysis of *Listeria monocytogenes* under pulsed magnetic field treatment. *Food Res. Int.* **2020**, *133*, 109195. [\[CrossRef\]](#) [\[PubMed\]](#)
- Guo, J.; Hu, X.; Gao, Z.; Li, G.; Fu, F.; Shang, X.; Liang, Z.; Shan, Y. Global transcriptomic response of *Listeria monocytogenes* exposed to Fingered Citron (*Citrus medica* L. var. *sarcodactylis* Swingle) essential oil. *Food Res. Int.* **2021**, *143*, 110274. [\[CrossRef\]](#) [\[PubMed\]](#)
- Yu, L.; Zhang, S.; Xu, Y.; Mi, X.; Xing, T.; Li, J.; Zhang, L.; Gao, F.; Jiang, Y. Acid resistance of *E. coli* O157:H7 and O26:H11 exposure to lactic acid revealed by transcriptomic analysis. *LWT-Food Sci. Technol.* **2021**, *136*, 110352. [\[CrossRef\]](#)
- Becavin, C.; Bouchier, C.; Lechat, P.; Archambaud, C.; Creno, S.; Gouin, E.; Zongfu, W.; Kuhbacher, A.; Brisse, S.; Pucciarelli, M.G.; et al. Comparison of widely used *Listeria monocytogenes* strains EGD, 10403S, and EGD-e highlights genomic differences underlying variations in pathogenicity. *MBio* **2014**, *5*, e00969-14. [\[CrossRef\]](#) [\[PubMed\]](#)

25. Fan, L.; Li, H.; Niu, Y.; Chen, Q. Characterization and Inducing Melanoma Cell Apoptosis Activity of Mannosylerythritol Lipids-A Produced from *Pseudozyma aphidis*. *PLoS ONE* **2016**, *11*, e0148198.
26. Kafantaris, I.; Tsadila, C.; Nikolaidis, M.; Tsavea, E.; Dimitriou, T.G.; Iliopoulos, I.; Amoutzias, G.D.; Mossialos, D. Transcriptomic Analysis of *Pseudomonas aeruginosa* Response to Pine Honey via RNA Sequencing Indicates Multiple Mechanisms of Antibacterial Activity. *Foods* **2021**, *10*, 936. [[CrossRef](#)]
27. Schmittgen, T.D.; Livak, K.J. Analyzing real-time PCR data by the comparative C-T method. *Nat. Protoc.* **2008**, *3*, 1101–1108. [[CrossRef](#)]
28. Dog-Hwan, O.; Marshall, D.L. Antimicrobial activity of ethanol, glycerol monolaurate or lactic acid against *Listeria monocytogenes*. *Int. J. Food Microbiol.* **1993**, *20*, 239–246.
29. Patro, R.; Mount, S.M.; Kingsford, C. Sailfish enables alignment-free isoform quantification from RNA-seq reads using lightweight algorithms. *Nat. Biotechnol.* **2014**, *32*, 462–464. [[CrossRef](#)]
30. Ledala, N.; Sengupta, M.; Muthaiyan, A.; Wilkinson, B.J.; Jayaswal, R.K. Transcriptomic Response of *Listeria monocytogenes* to Iron Limitation and fur Mutation. *Appl. Environ. Microb.* **2010**, *76*, 406–416. [[CrossRef](#)]
31. McLaughlin, H.P.; Hill, C.; Gahan, C.G.M. The impact of iron on *Listeria monocytogenes*; inside and outside the host. *Curr. Opin. Biotechnol.* **2011**, *22*, 194–199. [[CrossRef](#)] [[PubMed](#)]
32. Quistgaard, E.M.; Low, C.; Guettl, F.; Nordlund, P. Understanding transport by the major facilitator superfamily (MFS): Structures pave the way. *Nat. Rev. Mol. Cell Biol.* **2016**, *17*, 123–132. [[CrossRef](#)] [[PubMed](#)]
33. Gabrielsen, C.; Brede, D.A.; Hernandez, P.E.; Nes, I.F.; Diep, D.B. The Maltose ABC Transporter in *Lactococcus lactis* Facilitates High-Level Sensitivity to the Circular Bacteriocin Garvicin ML. *Antimicrob. Agents Chemother.* **2012**, *56*, 2908–2915. [[CrossRef](#)] [[PubMed](#)]
34. Lengeler, J.W.; Jahreis, K. Bacterial PEP-Dependent Carbohydrate: Phosphotransferase Systems Couple Sensing and Global Control Mechanisms. *Bact. Sens. Signal.* **2009**, *16*, 65–87.
35. Gabor, E.; Goehler, A.-K.; Kosfeld, A.; Staab, A.; Kremling, A.; Jahreis, K. The phosphoenolpyruvate-dependent glucose-phosphotransferase system from *Escherichia coli* K-12 as the center of a network regulating carbohydrate flux in the cell. *Eur. J. Cell Biol.* **2011**, *90*, 711–720. [[CrossRef](#)]
36. Metselaar, K.I.; den Besten, H.M.W.; Boekhorst, J.; van Hijum, S.A.F.T.; Zwietering, M.H.; Abee, T. Diversity of acid stress resistant variants of *Listeria monocytogenes* and the potential role of ribosomal protein S21 encoded by *rpsU*. *Front. Microbiol.* **2015**, *6*, 422. [[CrossRef](#)]
37. Wu, Y.; Pang, X.; Liu, X.; Wu, Y.; Zhang, X. Functional Genomics Identified Novel Genes Involved in Growth at Low Temperatures in *Listeria monocytogenes*. *Microbiol. Spectr.* **2022**, e00710-22. [[CrossRef](#)]
38. Ramakrishnan, V. Ribosome structure and the mechanism of translation. *Cell* **2002**, *108*, 557–572. [[CrossRef](#)]
39. Pechmann, S.; Willmund, F.; Frydman, J. The Ribosome as a Hub for Protein Quality Control. *Mol. Cell* **2013**, *49*, 411–421. [[CrossRef](#)]
40. Poehlsgaard, J.; Douthwaite, S. The bacterial ribosome as a target for antibiotics. *Nat. Rev. Microbiol.* **2005**, *3*, 870–881. [[CrossRef](#)]
41. Lin, J.; Zhou, D.; Steitz, T.A.; Polikanov, Y.S.; Gagnon, M.G. Ribosome-Targeting Antibiotics: Modes of Action, Mechanisms of Resistance, and Implications for Drug Design. *Annu. Rev. Biochem.* **2018**, *87*, 451–478. [[CrossRef](#)] [[PubMed](#)]
42. Saier, M.H., Jr. The Bacterial Phosphotransferase System: New Frontiers 50 Years after Its Discovery. *J. Mol. Microbiol. Biotechnol.* **2015**, *25*, 73–78. [[CrossRef](#)] [[PubMed](#)]
43. Tan, S.; Hua, X.; Xue, Z.; Ma, J. Cajanin Stilbene Acid Inhibited Vancomycin-Resistant Enterococcus by Inhibiting Phosphotransferase System. *Front. Pharmacol.* **2020**, *11*, 473. [[CrossRef](#)] [[PubMed](#)]
44. Snyder, H.; Kellogg, S.L.; Skarda, L.M.; Little, J.L.; Kristich, C.J. Nutritional Control of Antibiotic Resistance via an Interface between the Phosphotransferase System and a Two-Component Signaling System. *Antimicrob. Agents Chemother.* **2014**, *58*, 957–965. [[CrossRef](#)]
45. Huang, K.; Zeng, J.; Liu, X.; Jiang, T.; Wang, J. Structure of the mannose phosphotransferase system (man-PTS) complexed with microcin E492, a pore-forming bacteriocin. *Cell Discov.* **2021**, *7*, 1–5. [[CrossRef](#)]